MHD Flow in Curved Pipes Under a Nonuniform Magnetic Field

Chiara Mistrangelo and Leo Bühler

***Abstract*— In fusion reactors, a very hot deuterium–tritium plasma is confined in a toroidal volume by means of a strong magnetic field. In the blanket structure that surrounds the fusion plasma, high-energy neutrons, produced in the D-T fusion reaction, are absorbed by the lithium-containing liquid metal releasing their kinetic energy in the form of volumetric thermal load and breeding the fuel component tritium. The liquid metal flows from the blanket toward external ancillary systems for purification and tritium extraction. When the electrically conducting fluid moves in the strong plasma-confining magnetic field, induced electric currents generate electromagnetic Lorentz forces, which modify velocity distribution and increase pressure losses compared with hydrodynamic flows. These magnetohydrodynamic (MHD) effects have to be investigated to determine their impact on blanket performance. A number of studies on pressure -driven and buoyant MHD flows in geometries related to blanket modules are available, while only few works consider MHD flows in pipelines connecting blanket and ancillary systems. In the present study, we investigate numerically liquid metal MHD flows in the pipes, which cross the shield that protects the superconducting magnets from neutron radiation-induced damages. The geometry features two bends in series that turn the flow from the radial direction perpendicular to the magnetic field into a direction parallel to it and then back to a perpendicular orientation. The correct radial distribution of the magnetic field, as expected along the pipe axis, is taken into account. The flow experiences strong 3-D effects caused by Lorentz forces due to large-scale current loops driven by axial potential differences along the bend axis. In spite of very strong local MHD effects on velocity and pressure distribution, the overall pressure drop does not increase significantly compared with the one in a fully developed flow in a straight pipe of same length.**

***Index Terms*— Curved pipes, liquid metal blankets, magnetohydrodynamics (MHD), nonuniform magnetic field.**

I. Introduction

IN FUSION power reactors, a hot deuterium–tritium plasma is confined in a toroidal vacuum vessel by means of an imposed magnetic field. Lithium-containing liquid metals, such as the eutectic alloy lead lithium (PbLi), are foreseen as breeder material for in situ production of the fuel component tritium. Moreover, PbLi serves as a neutron multiplier, heat carrier, and coolant in blankets of future thermonuclear reactors. The blanket is the structure that faces the plasma on one side (first wall) and the protecting shield on the other side (back plates), as shown in Fig. 1, where the design of the ITER test blanket module (TBM) with pipelines is displayed [1]. The liquid metal from the blanket has to circulate toward ancillary systems for tritium extraction and purification. When the electrically conducting fluid moves in the strong magnetic field that confines the fusion plasma, electric currents are induced that generate electromagnetic Lorentz forces [2], which modify velocity distribution and increase pressure losses compared with hydrodynamic flow in the same geometry. These magnetohydrodynamic (MHD) effects have to be carefully analyzed to assess their impact on the performance of a fusion blanket. In recent years, a number of studies on pressure-driven and buoyant MHD flows in geometries related to blanket modules and in liquid metal manifolds enhanced the understanding of MHD phenomena in such components [3], [4], [5], [6], although the prediction of such flows in complete blanket modules for fusion relevant parameters is still ongoing [7]. On the other hand, only few works [8], [9] considered the MHD flow in supply and return pipe lines connecting the blanket modules with the ancillary systems, and to the best of our knowledge, bend flows in nonuniform magnetic fields, as present in ITER, have not been considered so far.

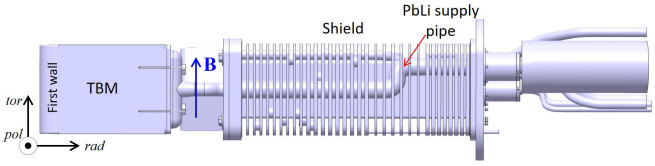

Fig. 1. View on the ITER TBM and the PbLi pipes across the shield [1].

In the present work, we investigate the liquid metal flows in the pipes which cross the shield that protects the superconducting magnets from neutron radiation-induced damages and associated heating. The supplying pipe features two bends in series that turn the flow from the radial direction perpendicular to the toroidal magnetic field **B** into a direction parallel to it and then back to a perpendicular orientation (Fig. 1). In fully developed MHD flows in straight pipes in uniform magnetic fields, electric currents close within duct cross sections remaining confined in 2-D planes parallel to the magnetic field.

Manuscript received 21 August 2023; revised 22 December 2023; accepted 17 January 2024. This work was supported by the Framework of the EUROfusion Consortium, funded by the European Union via the Euratom Research and Training Program under Grant 101052 200 — EUROfusion. The review of this article was arranged by Senior Editor R. Chapman. *(Corresponding author: Chiara Mistrangelo.)*

The authors are with the Karlsruhe Institute of Technology, 76021 Karlsruhe, Germany (e-mail: chiara.mistrangelo@kit.edu; leo.buehler@kit.edu).

Color versions of one or more figures in this article are available at https://doi.org/10.1109/TPS.2024.3358018.

Digital Object Identifier 10.1109/TPS.2024.3358018

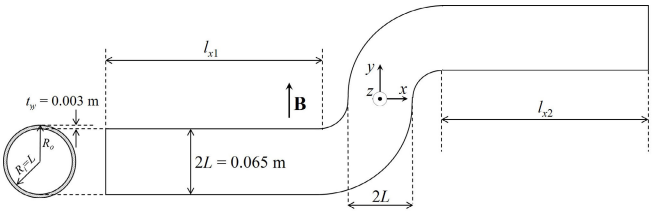

Fig. 2. Model geometry used for the numerical analysis, coordinate system, and main dimensions. The pipe has an inner diameter of $2L = 0.065$ m and a wall with thickness $t_w = 0.003$ m.

TABLE I
OPERATING CONDITIONS OF THE WCLL TBM AND MODEL DIMENSIONS

L	t_w	$\dot{m}$	$u_0 = \frac{\dot{m}}{\rho\pi L^2}$	T_{in}	T_{out}	T_0
mm	mm	$\frac{\text{kg}}{\text{s}}$	$\frac{\text{m}}{\text{s}}$	°C	°C	°C
32.5	3	0.65	1.99×10^{-2}	295	319	307

In curved geometries, axial potential gradients occur that drive currents along 3-D loops traversing different cross-sectional planes. These currents induce electromagnetic Lorentz forces that affect velocity and pressure distribution in the double-bend pipe considered in the present study [9]. In the problem under investigation, we take into account additionally the influence of a realistic magnetic field that varies spatially along the radial direction (see Fig. 3).

II. Model Geometry

In Fig. 2, the model geometry is displayed together with the used coordinate system that is centered in the middle of the double bend. The dimensions of the pipes connecting the WCLL TBM to the ancillary systems have been taken from the most recent design for ITER. As for previous numerical studies, where the magnetic field was assumed constant across the shield [9], operating conditions have been provided by Fusion for Energy (F4E), which is the EU organization managing Europe's contribution to ITER, and the data used for the present simulations are summarized in Table I.

For applications in ITER, the magnetic field across the shield is not uniform and its radial distribution is plotted in Fig. 3. The solid lines indicate the distribution of the toroidal magnetic field at different poloidal positions, as provided by F4E. The red dashed line is obtained by fitting the curves in the region of interest and this distribution is used for the numerical simulations. The focus of the present simulations is on MHD flow in the bends, the center of which is located at $X = 2.369$ m. The positions of the model geometry in the spatially varying magnetic field and colored contours of B are shown in the subplot on the top left of the figure. Over a sufficiently long range upstream and downstream of these bends, the magnetic field is well-approximated by the used fitting function across the entire shield (see the sketch on the bottom of Fig. 3 showing the position of TBM and shield). Since the numerical simulations require well-defined entrance and exit boundary conditions, it is assumed that the magnetic field is constant in a certain portion of the inlet and the outlet pipes at sufficient distance from the bends.

III. Governing Equations and Flow Parameters

We consider the incompressible, viscous, MHD flow of an electrically conducting fluid, such as a liquid metal, exposed

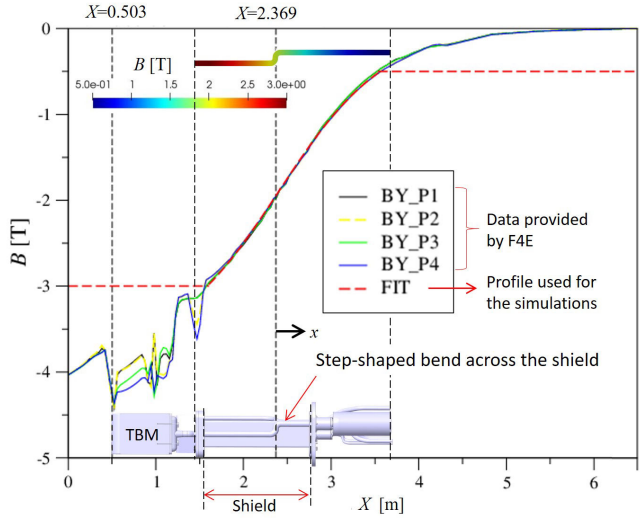

Fig. 3. Radial distribution of the magnetic field. Solid lines represent calculated distribution of the toroidal magnetic field taken at different poloidal positions. The red dashed line is a fitting curve used for the numerical calculations in the present study. Contours of magnetic field strength in the model geometry are shown in the subplot on the top left side of the figure.

to an externally applied magnetic field, which is governed by equations for balance of momentum, conservation of mass, where currents are calculated by Ohm's law

$$\rho\left(\frac{\partial}{\partial t} + \mathbf{v}\cdot\nabla\right)\mathbf{v} = -\nabla p + \rho\nu\nabla^2\mathbf{v} + \mathbf{j}\times\mathbf{B} \quad (1)$$

$$\nabla\cdot\mathbf{v} = 0,\ \ \mathbf{j} = \sigma(-\nabla\phi + \mathbf{v}\times\mathbf{B}). \quad (2)$$

Here, $\mathbf{v}$, $\mathbf{j}$, $\mathbf{B}$, and ϕ stand for the velocity, current density, applied magnetic flux density, and electric potential, respectively. The physical properties of the fluid, density ρ, kinematic viscosity ν, and electric conductivity σ, are assumed to be constant and taken at the mean temperature $T_0 = 307$ °C (Table I) from the material database reviewed in [10] (Table II).

The electric potential ϕ is determined by a Poisson equation obtained by combining Ohm's law (2) with the condition for charge conservation $\nabla\cdot\mathbf{j} = 0$

$$\nabla^2\phi = \nabla\cdot(\mathbf{v}\times\mathbf{B}). \quad (3)$$

In the wall, this equation reduces to $\nabla^2\phi_w = 0$.

The flow is characterized by two dimensionless parameters, the Hartmann number, Ha, and the Reynolds number, Re

$$\text{Ha} = B_0 L\sqrt{\frac{\sigma}{\rho\nu}},\ \text{Re} = \frac{u_0 L}{\nu}. \quad (4)$$

The former one gives a nondimensional measure for the strength B_0 of the imposed magnetic field and its square describes the ratio between electromagnetic and viscous forces. The Reynolds number indicates the ratio of inertia to viscous forces and can also be expressed as $\text{Re} = \text{Ha}^2/\text{N}$, where $\text{N} = \sigma L B_0^2/(\rho u_0)$ is the interaction parameter. The typical length scale of the problem L is the internal radius R_i of the pipe (see Fig. 2) and the characteristic velocity u_0 is chosen as the mean velocity in the pipe. Equations are formulated according to the inductionless or quasi-static

TABLE II
MATERIAL PROPERTIES OF PBLI [10] AND OF WALL MATERIAL [15] AT 307 °C

PbLi				Wall
ρ	μ	$\nu=\mu/\rho$	σ	σ_w
$\frac{\mathrm{kg}}{\mathrm{m}^3}$	$\frac{\mathrm{kg}}{\mathrm{ms}}$	$\frac{\mathrm{m}^2}{\mathrm{s}}$	$\frac{1}{\Omega\mathrm{m}}$	$\frac{1}{\Omega\mathrm{m}}$
9830	1.22×10^{-3}	1.24×10^{-7}	8.81×10^{5}	1.18×10^{6}

approximation, which is valid at low magnetic Reynolds number, $\mathrm{Re}_m = \mu\sigma L u_0 = 3\cdot10^{-3}$ (for $u_0 = 0.1$ m/s) $\ll 1$, where μ is the magnetic permeability. It states that the magnetic field induced by currents in the fluid is negligible compared with the externally applied field $\mathbf{B}$ [11], [12].

As kinematic boundary conditions at the wall, the no-slip condition, $\mathbf{v} = 0$, is applied. The external surface of the wall is electrically insulating, $\partial\phi_w/\partial n = 0$, and at the fluid–wall interface the flow satisfies continuity of electric potential and normal component of current density, $\phi = \phi_w$ and $j_n = j_{nw}$, i.e., there is no contact resistance. At the inlet of the pipe, no axial currents, i.e., $\partial\phi/\partial x = 0$, a uniform magnetic field B_0, and velocity u_0, are imposed. The conductance of the wall with specific conductivity σ_w and thickness t_w compared with the one of the fluid is described by the wall conductance ratio c. This parameter can be defined according to two different formulations, one applies for circular pipes with walls of arbitrary thickness [13] and the other one is more general in terms of geometry but only valid for thin walls, $t_w \ll L$ [14]

$$c_M = \frac{\sigma_w}{\sigma}\frac{R_o^2 - R_i^2}{R_o^2 + R_i^2} = 0.1175, \quad c_W = \frac{\sigma_w t_w}{\sigma L} = 0.123. \tag{5}$$

For the operating conditions defined in Table I, a maximum magnetic field of 3T and the material properties given in Table II nondimensional parameters characterizing the MHD pipe flow across the shield become Ha = 2621, N = 1318, and the hydrodynamic Reynolds number based on L is $\mathrm{Re} = \mathrm{Ha}^2/\mathrm{N} = 5215$. Hydrodynamic flows at comparable Reynolds numbers are expected to be turbulent. However, for strong magnetic fields (large Ha), the MHD flow becomes laminar, since inertia forces are negligible compared with the strong electromagnetic forces (large N) [16], [17]. The MHD flow in the core is mainly governed by a balance between pressure and electromagnetic Lorentz forces, while viscous forces are important only in the thin boundary layers along walls.

Numerical simulations are performed by means of a finite volume solver implemented in the frame of the open source code OpenFOAM. A cell-centered finite volume method is used to discretize the equations. A segregated solver is employed, and for the coupling between pressure and velocity the pressure implicit with splitting of operators (PISO) algorithm available in OpenFOAM is applied. The Lorentz force is treated explicitly and defined at cell centers. Required centroid currents are obtained by interpolation from face current fluxes using the identity $\mathbf{j} = \nabla\cdot(\mathbf{jr})$, where $\mathbf{r}$ is the distance vector [18], [19], to avoid spurious contributions to the electromagnetic force due to discretization errors. The standard Gaussian finite volume integration is used for discretization of convective terms, together with a second order skewness-corrected interpolation scheme required when using nonorthogonal meshes as in the present study.

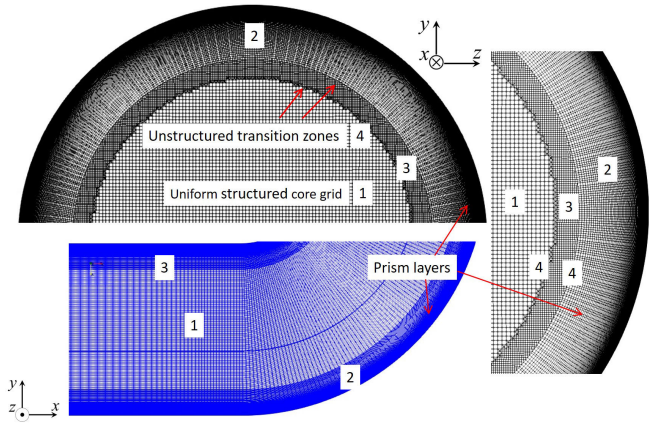

Fig. 4. Example of mesh used to discretize the fluid domain in the bends. The mesh consists of regions that are topologically different. There is a uniform structured core grid (1), wall-aligned prism layers to resolve the near-solid region (2) and the wall, and unstructured transition meshes to join the various zones (4).

In addition to numerical simulations by OpenFOAM, asymptotic analyses are performed that are valid for $\mathrm{Ha} \gg 1$ and $\mathrm{N} \to \infty$, i.e., for strong magnetic fields and neglecting inertia effects. These results obtained using boundary fit coordinates, as described in [20], are compared with the present full numerical simulations.

IV. COMPUTATIONAL MESH

Different types of computational meshes have been tested to find the most suitable one for the prediction of MHD flows exposed to strong magnetic fields in arbitrary geometries. A number of software have been considered for automatic generation of the grid and also the topology of the cells have been varied. The performance of the code when using hexa-, poly-, and tetrahedral elements has been investigated. Most accurate results have been obtained using hex-dominant meshes with thin prism elements in boundary regions. Best performance and suppression of numerical instabilities and disturbances require additionally the use of corrections for the calculation of gradients, especially for the electric potential, when using meshes with nonorthogonal cells. The nonorthogonality of a grid is defined as the angle formed by the vector connecting two adjacent cell centers and the vector normal to the shared face. In case of orthogonal meshes, the angle is zero since the face normal and the center joining vectors are aligned.

Fig. 4 shows details of the mesh in the fluid domain used for the solution of the present problem. The mesh in the pipe cross section is characterized by a uniform structured core region (1) and wall-parallel prism layers (2) closer to the solid domain and in the wall. It has been observed that the presence of an additional uniform structured zone (3) for the transition between the mesh portions (1) and (2) leads to more stable simulation runs. The various structured grids are joined by thin unstructured layers (4). The number of these irregular cells has been minimized and their position has been shifted to a certain distance from the boundary regions in which larger variable gradients are expected.

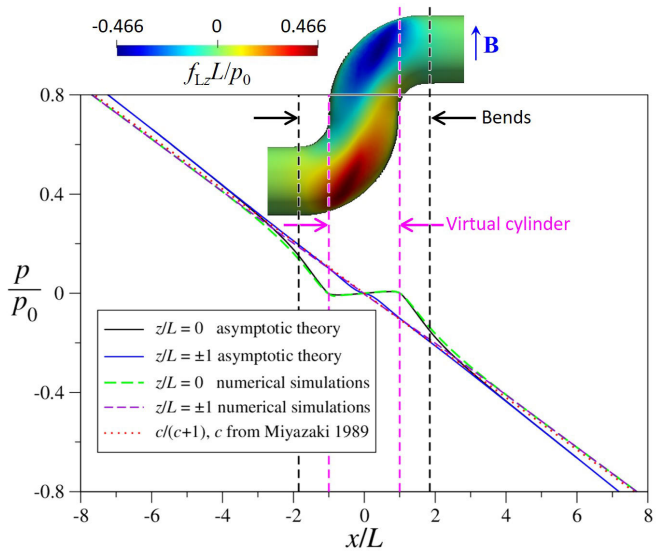

Fig. 5. Scaled pressure plotted along the axial direction for a uniform magnetic field $B = 3$ T. Solid lines are the results from an asymptotic solution valid for large Ha and N $\to \infty$, and the dashed lines are obtained by full numerical simulations. On the top of the figure, color contours of the transverse component of the Lorentz force density f_{Lz} normalized by p_0/L are displayed on the bend surface.

V. Numerical Results

Before performing full numerical simulations in the nonuniform magnetic field $B(x)$ as present across the shield, simulations for a uniform field $B = 3$ T have been carried out and compared with the asymptotic results to test the problem setup and code performances for such MHD flow. In Fig. 5, the pressure normalized by $p_0 = \sigma L u_0 B^2$ is plotted along the scaled axial coordinate of the geometry both in the middle ($z/L = 0$) and near the side walls ($z/L = \pm 1$) of the ducts. It can be seen that asymptotic results valid for large Ha and N $\to \infty$ (solid lines) and full numerical simulations (dashed lines) exhibit quite good agreement for pressure variation in the 3-D region of the geometry. We find increased pressure gradients when entering and leaving the bends and a weak locally reversed pressure gradient in the center of the step-shaped duct inside a virtual cylinder. The latter is bordered by internal layers that develop parallel to the magnetic field and tangent to the bend walls. A more detailed description of this peculiar region is given in the following when describing results for the MHD flow in a nonuniform $B(x)$. The results of 3-D numerical simulations show slightly smaller pressure gradients in fully developed flow regions at some distance from the bends compared with the asymptotic solution. This can be explained by the fact that the latter analysis uses the definition c_W of the wall conductance parameter (5) according to Walker [14] that assumes that walls are very thin, $t_w \ll L$. Instead, the numerical approach resolves the finite thickness of the wall with a fine grid. In Fig. 5, the red dotted line corresponds to the theoretically predicted constant pressure gradient in fully developed pipe flow, $\partial_x p = -c_M/(c_M + 1)$, whose validity is not restricted to thin walls [13]. This formulation agrees well with the numerical results and confirms together with the asymptotic results the quality of the used mesh and the correct implementation of algorithms and numerical schemes for nonorthogonal meshes.

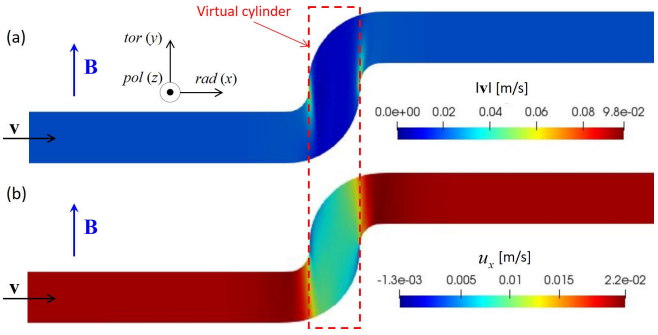

Fig. 6. Results for Ha = 2621 and N = 1318. Contours of (a) velocity magnitude and (b) axial velocity on the vertical symmetry plane at $z = 0$. The red dashed line marks the virtual cylinder.

The color plot on the top of Fig. 5 shows on the fluid–wall interface contours of the transverse component of the Lorentz force f_{Lz} scaled by p_0/L. These forces are responsible for the pressure difference between the center of the bend ($z/L = 0$) and the sides ($z/L = \pm 1$).

In the following, the results are presented for the geometry described in Fig. 2 and the magnetic field distribution as plotted in Fig. 3. We consider a double-curved pipe with a radial–toroidal–radial orientation, which transports the liquid metal from the region with large magnetic field, i.e., from the blanket, toward the ancillary systems where B is much smaller.

Fig. 6 shows contours of (a) velocity magnitude and (b) axial velocity on the vertical symmetry plane at $z = 0$. The strongest velocity gradients occur across the thin internal layer that develops along magnetic field lines tangent to the wall of the double bend. Together with the boundary layers, it forms a virtual cylinder, marked by the red dashed line, in the periphery of which the 3-D MHD phenomena are mainly confined. The tangent cylinder emerges from the line on the geometry where $\mathbf{B} \cdot \mathbf{n} = 0$ and it spreads through the fluid along magnetic field lines. In this sense, it is comparable to internal Ludford layers that develop likewise in the fluid, originating from singularities in the geometry [21]. Those layers are also closely related to the characteristic surfaces introduced by [22].

The contours of the axial velocity component [Fig. 6(b)] clearly show that the fluid domain splits into three cores: those upstream and downstream the bends have similar characteristics, and the velocity distribution is pretty uniform resembling the main features of a fully developed velocity profile. In the middle core, the velocity in the center reduces significantly, while the largest portion of the flow rate is transported by boundary and internal layers where high-velocity jets are present. The evolution of the velocity distribution and the progressive growth of the velocity magnitude in the layers can be seen in Fig. 7 in which 3-D velocity profiles, colored by the velocity magnitude, are plotted at different axial positions. The red velocity streamlines in Fig. 7 show the exchange of flow between internal layers.

The origin of the 3-D MHD effects in the region close to the bends can be explained by looking at the distribution of the electric potential, as shown in Fig. 8. On the top (a),

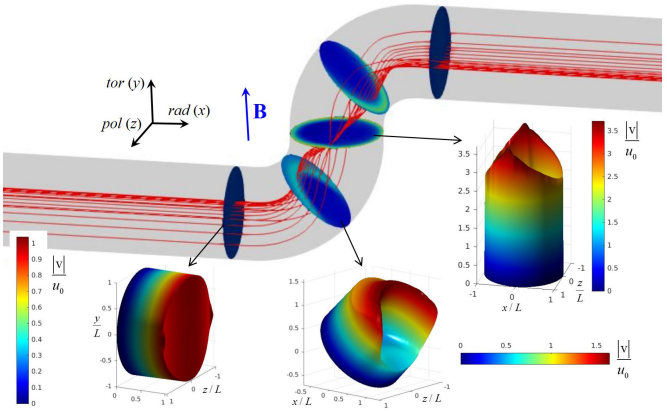

Fig. 7. Results for Ha = 2621 and N = 1318. Three-dimensional velocity distribution at different axial positions. When approaching the bends, the velocity starts increasing in the boundary layers while reducing in the center. Red velocity streamlines indicate how the flow moves across the bend center from one internal layer to the other one.

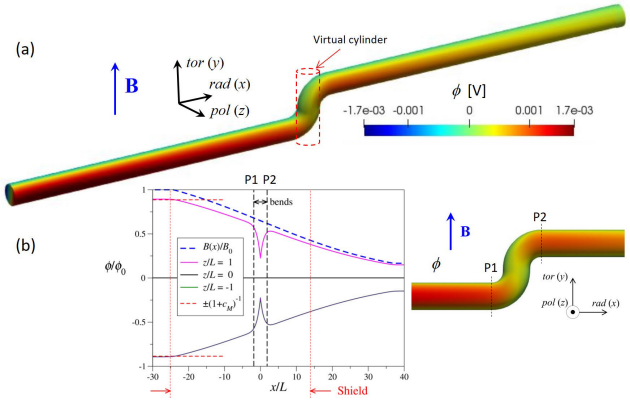

Fig. 8. Results for Ha = 2621 and N = 1318. (a) Contours of electric potential and (b) its axial variation in the center of the geometry ($z/L = 0$) and near the sides ($z/L = \pm 1$). The two vertical red lines in (b) indicate the length of the shield. The figure on the right shows the beginning (P1) and the end (P2) of the bends.

colored contours of electric potential are plotted on the fluid–wall interface. The strongest axial potential gradients are localized near the virtual cylinder indicated by the red dashed lines. Moderate axial potential variations are also present in the straight pipes caused by the radial profile of the magnetic field $B(x)$. Only in the regions where the magnetic field is assumed constant, at sufficient distance from the bends, where fully developed conditions are reached, the potential is constant along x with changes only in the transverse z direction. The axial profiles of electric potential in the center of the geometry ($z/L = 0$) and near the sides ($z/L = \pm 1$) are plotted in Fig. 8(b). Highest values of potential magnitude are found near the sides in the inlet region, where the electric potential scaled by $\phi_0 = u_0 B L$ is $(\phi/\phi_0)(x = -\infty, z/L = \pm 1) = \pm 0.894$. This value is in agreement with predictions for fully developed flow in electrically conducting pipes [13], where $(\phi/\phi_0)_{FD}(z/L = \pm 1) = \pm(1 + c_M)^{-1} = 0.8948$, with conductance parameter $c_M = 0.1175$ (5). When approaching the bends, a significant local reduction in the magnitude of wall potential can be observed near the sides at $z/L = \pm 1$. In Fig. 8(b), cross sections at positions P1 and P2 indicate the beginning and the end of the bends (see figure on the right).

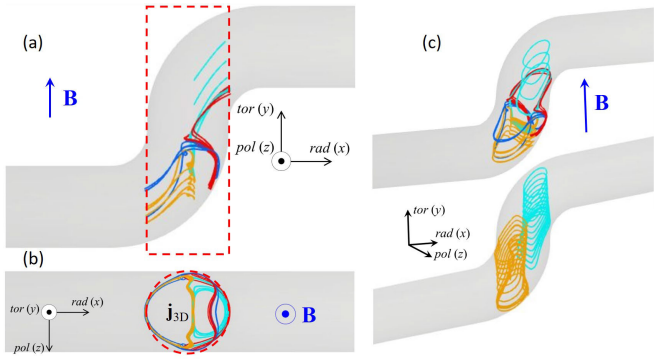

Fig. 9. Results for Ha = 2621 and N = 1318. Electric current streamlines that close exclusively in the fluid. The red dashed line indicates the virtual cylinder.

The axial variations in electric potential drive axial currents that close through the wall and the fluid giving rise to 3-D electric currents $\mathbf{j}_{3-D}$ and Lorentz forces $\mathbf{f}_L$ that affect velocity and pressure distribution. In the identified virtual cylinder, the 3-D currents close exclusively in the fluid domain. In Fig. 9, some characteristic current streamlines are displayed. (a) Side, (b) top, and (c) 3-D views should facilitate the understanding of the complex current paths. The orange and cyan lines form two vortex tubes elongated in the toroidal direction (Fig. 9(c) on the bottom) which meet almost in the center of the virtual cylinder (b). In the lower part of the bends, there are current lines that circulate across the entire cross section of the virtual cylinder (blue lines), and in the right half the red lines follow partly the bend wall and then turn upstream forming larger loops.

When seeding the current streamlines in the external periphery of the virtual cylinder, currents induced in the fluid close their path through the wall, as visible in Fig. 10 (blue lines). Here different views show how the current flows in the wall, where a saddle point can be identified near the middle of the bends in the side walls $z/L = \pm 1$. Orange and cyan current lines circulate only in the fluid as displayed in Fig. 9. These streamlines are also plotted here to clarify the position of the virtual cylinder compared with the blue current lines. In Fig. 10(c) on the bottom, red current lines outside the bends in the straight pipes exhibit as well a certain axial component due to the spatial gradient in the magnetic field distribution. However, in these pipes the 3-D MHD effects are much weaker than in the bends. In the regions at the inlet and outlet of the geometry (not visible in Fig. 10), where the magnetic field is assumed constant, fully developed conditions are reached and currents circulate there in 2-D cross-sectional planes.

The axial variation in pressure along lines in the center of the geometry at $z/L = 0$ and near the sides at $z/L = \pm 1$ is plotted in Fig. 11. The pressure has been scaled by the quantity $p_0 = \sigma u_0 B^2 L$. The two vertical dashed lines indicate the position of the shield behind the ITER TBM (see figure on the bottom) and $x/L = 0$ is the middle of the step. For better visualization, the distribution in the center has been enlarged in the subplot on the right-hand side. Near the sides at $z/L = \pm 1$, 3-D MHD effects are weaker than in the middle of the pipes since transverse Lorentz forces compensate the stronger axial gradients in the center. Solid lines are the results obtained by

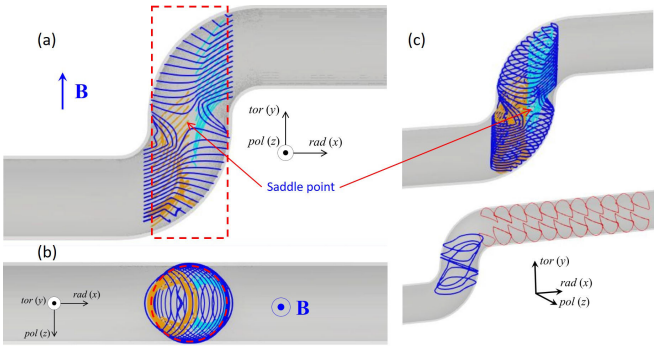

Fig. 10. Results for Ha = 2621 and N = 1318. Blue and red current streamlines close also in the wall. The current paths in the fluid (orange and cyan) are the same as in Fig. 9(c).

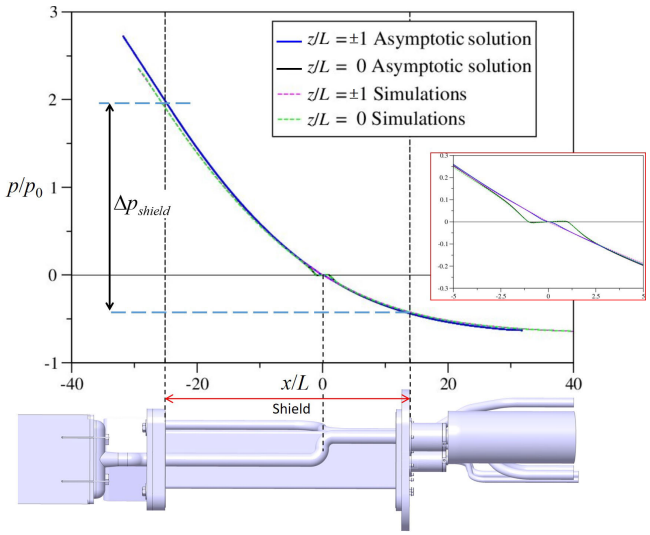

Fig. 11. Results for Ha = 2621 and N = 1318. Scaled pressure plotted along the axial direction. On the right in the subplot, the distribution in the bends has been enlarged for better visualization. Solid lines are the results from an asymptotic solution valid for Ha $\gg$ 1 and N $\to \infty$, and the dashed lines are obtained by full numerical simulations.

an asymptotic approach valid for Ha $\gg$ 1 and N $\to \infty$, while the dashed lines are from full numerical simulations. The two sets of data evidence a very good agreement, indicating that inertia forces are unimportant. When increasing the flow rate, inertia forces become stronger and weak deviations from the inertialess solution are visible in the middle of the bends.

In Fig. 12, the axial pressure gradient scaled by p_0/L is plotted along the normalized coordinate x/L. Close to the inlet and the outlet of the geometry, where the magnetic field is assumed constant, the flow reaches fully developed conditions characterized by a constant pressure gradient. The dot-dashed line indicates the theoretical value $\partial_x p = -c_M/(c_M + 1)$ for fully established pipe flow [13]. While the magnetic field $B(x)$ becomes smaller along the radial direction, the magnitude of the pressure gradient reduces progressively as well. When the flow approaches the step, the magnitude of the pressure gradient starts increasing rapidly up to a local maximum before reducing abruptly and becoming even reversed within the bend region. Similar phenomena are observed behind the bends, where another local maximum occurs. Afterward, the pressure gradient decreases and it recovers the expected fully

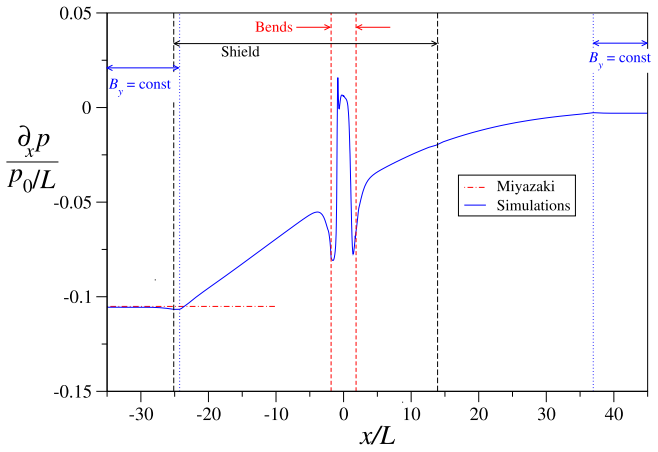

Fig. 12. Radial pressure gradient $\partial_x p$ along the center of the pipe, normalized by p_0/L. Results are plotted along the scaled coordinate x/L for Ha = 2621 and N = 1318. The horizontal dot-dashed line indicates the theoretical solution for fully developed flow according to [13].

developed flow value in the outlet duct where the magnetic field is assumed constant. This faster axial variation in the pressure near the bends for $-5 < x/L < 5$ is due to the occurrence of 3-D currents (see Fig. 9) that create additional electromagnetic Lorentz forces, which influence locally the pressure distribution. It can be observed that the presence of the bends causes significant 3-D MHD effects which, however, remain confined to the region immediately around the bends where they affect mainly the local velocity distribution.

VI. Conclusion

Numerical simulations of liquid metal MHD flows in double bends with circular cross section, as those foreseen across the radiation shield behind the ITER TBM, have been performed for a realistic distribution $B(x)$ of the toroidal magnetic field. The latter varies in the radial direction from a value of $B \approx 3$T near the back plate of the TBM to much smaller values at the far end of the shield. The results have been obtained using a realistic distribution of $B(x)$ according to the input data provided by F4E (Fig. 3).

Due to the nonuniform magnetic field $B(x)$, the pressure drops along x approximately as $\partial_x p(x) \sim B^2(x)$, which leads to a rapid decrease in pressure along the radial coordinate x. However, since the variation in B along x happens over a longer distance compared with the pipe diameter, 3-D effects in the straight pipes remain moderate and the flow at a certain distance from the bends resembles a locally quasi fully developed flow with almost uniform core velocity and only slight local overspeed in the Roberts layers that form near the walls whose normal vector is perpendicular to the magnetic field [23]. Close to the bends, strong 3-D modifications occur in all the variables such as pressure, velocity, electric potential, and currents. In the bends, the flow is carried preferentially in thin parallel internal layers that create a virtual tangent cylinder aligned with magnetic field lines.

In the core of the virtual cylinder, the velocity is very small. Electric currents prefer not to cross this cylinder and they either stay in its central core or flow around it. The pressure distribution inside the virtual cylinder shows a plateau and it has even a slightly reversed radial gradient. This effect

TABLE III
PARAMETRIC STUDY: INFLUENCE OF REYNOLDS NUMBER ON TOTAL PRESSURE DROP $\triangle p_{shield}$ ACROSS THE SHIELD

$\dot{m}$	u_0	Δp_{shield}	Re	Ha
kg/s	m/s	bar		
0.6498	0.02	0.12	5220	2621
1.625	0.05	0.3	13050	2621
3.25	0.10	0.6	26100	2621

compensates practically the increased pressure drop upstream and downstream of the bends that is caused by Lorentz forces originating from additional 3-D currents. The total pressure drop along the entire shield has been determined and quantified as nondimensional quantity Δp_{shield} (see Fig. 11). The results for ITER parameters, i.e., $\dot{m} = 0.6498$ kg/s, $u_0 = 0.02$ m/s, and $B(x)$, according to Fig. 3 with $B_0 = 3$T, yield a total pressure drop $\Delta p_{shield} = 0.12$ bar. Values of pressure drop for higher velocities are displayed in Table III, and they are in perfect agreement with data from the asymptotic theory.

ACKNOWLEDGMENT

This work has been carried out within the framework of the EUROfusion Consortium, funded by the European Union via the Euratom Research and Training Programme (Grant Agreement 101052 200 — EUROfusion). Views and opinions expressed are however those of the author(s) only and do not necessarily reflect those of the European Union or the European Commission. Neither the European Union nor the European Commission can be held responsible for them.

REFERENCES

[1] J. Aubert et al., "Design and preliminary analyses of the new water cooled lithium lead TBM for ITER," *Fusion Eng. Design*, vol. 160, Nov. 2020, Art. no. 111921.
[2] O. Lielausis, "Liquid-metal magnetohydrodynamics," *At. Energy Rev.*, vol. 13, no. 3, pp. 527–581, 1975.
[3] Y. Yan, A. Ying, and M. Abdou, "Numerical study of magneto-convection flows in a complex prototypical liquid-metal fusion blanket geometry," *Fusion Eng. Design*, vol. 159, Oct. 2020, Art. no. 111688.
[4] L. Chen, S. Smolentsev, and M.-J. Ni, "Toward full simulations for a liquid metal blanket: MHD flow computations for a PbLi blanket prototype at $Ha \sim 10^4$," *Nucl. Fusion*, vol. 60, no. 7, Jul. 2020, Art. no. 076003.
[5] L. Bühler and C. Mistrangelo, "A simple MHD model for coupling poloidal manifolds to breeder units in liquid metal blankets," *Fusion Eng. Design*, vol. 191, Jun. 2023, Art. no. 113552.
[6] O. Zikanov, I. Belyaev, Y. Listratov, P. Frick, N. Razuvanov, and V. Sviridov, "Mixed convection in pipe and duct flows with strong magnetic fields," *Appl. Mech. Rev.*, vol. 73, no. 1, Jan. 2021, Art. no. 010801.
[7] C. Mistrangelo, L. Bühler, V. Klüber, and C. Koehly, "Towards the simulation of MHD flow in an entire WCLL TBM mock-up," *Fusion Eng. Design*, vol. 193, Aug. 2023, Art. no. 113752.
[8] A. Tassone, G. Caruso, and A. Del Nevo, "Influence of PbLi hydraulic path and integration layout on MHD pressure losses," *Fusion Eng. Design*, vol. 155, Jun. 2020, Art. no. 111517.
[9] L. Bühler, V. Klüber, and C. Mistrangelo, "Magnetohydrodynamic flow in stepwise bent circular pipes," *Magnetohydrodynamics*, vol. 58, no. 4, pp. 339–347, 2022.
[10] D. Martelli, A. Venturini, and M. Utili, "Literature review of lead-lithium thermophysical properties," *Fusion Eng. Design*, vol. 138, pp. 183–195, Jan. 2019.
[11] H. Branover, *Magnetohydrodynamic Flow in Ducts*. New York, NY, USA: Wiley, 1978.
[12] R. Moreau, *Magnetohydrodynamics*. Norwell, MA, USA: Kluwer Academic, 1990.
[13] K. Miyazaki, S. Inoue, and N. Yamaoka, "MHD pressure drop of liquid metal flow in circular and rectangular ducts under transverse magnetic field," in *Liquid Metal Magnetohydrodynamics*, J. Lielpeteris and R. Moreau, Eds. Norwell, MA, USA: Kluwer, 1989, pp. 29–36.
[14] J. S. Walker, "Magnetohydrodynamic flows in rectangular ducts with thin conducting walls," *J. de Mécanique*, vol. 20, no. 1, pp. 79–112, 1981.
[15] K. Mergia and N. Boukos, "Structural, thermal, electrical and magnetic properties of Eurofer 97 steel," *J. Nucl. Mater.*, vol. 373, nos. 1–3, pp. 1–8, Feb. 2008.
[16] X. Albets-Chico, D. G. E. Grigoriadis, E. V. Votyakov, and S. Kassinos, "Direct numerical simulation of turbulent liquid metal flow entering a magnetic field," *Fusion Eng. Design*, vol. 88, no. 12, pp. 3108–3124, Dec. 2013.
[17] V. Klüber, L. Bühler, and C. Mistrangelo, "Numerical simulation of 3D magnetohydrodynamic liquid metal flow in a spatially varying solenoidal magnetic field," *Fusion Eng. Design*, vol. 156, Jul. 2020, Art. no. 111659.
[18] M.-J. Ni, R. Munipalli, N. B. Morley, P. Huang, and M. A. Abdou, "A current density conservative scheme for incompressible MHD flows at a low magnetic Reynolds number. Part I: On a rectangular collocated grid system," *J. Comput. Phys.*, vol. 227, no. 1, pp. 174–204, Nov. 2007.
[19] M.-J. Ni, R. Munipalli, P. Huang, N. B. Morley, and M. A. Abdou, "A current density conservative scheme for incompressible MHD flows at a low magnetic Reynolds number. Part II: On an arbitrary collocated mesh," *J. Comput. Phys.*, vol. 227, no. 1, pp. 205–228, Nov. 2007.
[20] L. Bühler, "Magnetohydrodynamic flows in abitrary geometries in strong, nonuniform magnetic fields," *Fusion Technol.*, vol. 27, no. 1, pp. 3–24, 1995.
[21] J. C. R. Hunt and G. S. S. Ludford, "Three-dimensional MHD duct flows with strong transverse magnetic fields Part 1. Obstacles in a constant area channel," *J. Fluid Mech.*, vol. 33, no. 4, p. 693, Sep. 1968.
[22] J. S. Walker and G. S. S. Ludford, "MHD flow in conducting circular expansions with strong transverse magnetic fields," *Int. J. Eng. Sci.*, vol. 12, no. 3, pp. 193–204, Mar. 1974.
[23] J. A. Shercliff, "Magnetohydrodynamic pipe flow Part 2. High Hartmann number," *J. Fluid Mech.*, vol. 13, no. 4, pp. 513–518, Aug. 1962.

Chiara Mistrangelo received the Ph.D. degree in fluid dynamics from Karlsruhe University, Karlsruhe, Germany, in 2005.

She is a Senior Researcher and a Lecturer at the Department for Thermal Energy Technology and Safety, KIT. Her current research interests include pressure-driven and buoyancy-driven convective MHD flows in complex geometries, code development, and validation through experiments and benchmark activities.

Leo Bühler received the Dr.-Ing. and Habilitation degrees in fluid dynamics from Karlsruhe University, Karlsruhe, Germany, in 1992 and in 2008, respectively.

He is a Professor at the Department for Thermal Energy Technology and Safety, KIT and the Head of the MHD Research Group, MEKKA and MaPLE facilities. His research interests include any kind of MHD flow in generic and complex geometries, asymptotic analysis, code development, and validation through experiments.